Available online at www.sciencedirect.com

ScienceDirect

Scripta Materialia xxx (2015) xxx–xxx

Scripta MATERIALIA

www.elsevier.com/locate/scriptamat

Kinetics of hydrogen reduction of titanium-doped molybdenum dioxide

Qian He,[a,*] Oscar Marin-Flores,[a] Shuozhen Hu,[b] Louis Scudiero,[c] Su Ha[b] and M. Grant Norton[a,*]

[a]*The School of Mechanical and Materials Engineering, Washington State University, Pullman, WA 99164, USA*
[b]*The Gene and Linda Voiland School of Chemical Engineering and Bioengineering, Washington State University, Pullman, WA 99164, USA*
[c]*Department of Chemistry, Washington State University, Pullman, WA 99164, USA*

Received 28 October 2014; accepted 15 December 2014

Ti-doped MoO_2 was synthesized to broaden the oxygen-to-carbon ratio operating range of MoO_2 for partial oxidation of long-chain hydrocarbons by increasing the redox stability. The structure modification causes the hydrogen reduction mechanism to change from three-dimensional nuclei growth with an activation energy of 61.3 kJ mol^{-1} to a three-dimensional hydrogen diffusion limited model with an activation energy of 317.9 kJ mol^{-1}. Because of the enhanced redox stability, Ti-doped MoO_2 has potential as an alternative anode in direct liquid-fed solid oxide fuel cells.

Keywords: Ti-doped MoO_2; Hydrogen reduction mechanism; Activation energy; Kinetics

The use of MoO_2, a transition metal oxide, as a catalyst with high activity, excellent coking resistance and sulfur tolerance for the partial oxidation of liquid hydrocarbons has been previously reported by our group [1–5]. We have also demonstrated the use of MoO_2 as an anode for solid oxide fuel cells (SOFCs) [6–8]. Because MoO_2 has mixed ionic and electronic conductivity, as well as high catalytic activities toward the reforming of long chain hydrocarbon fuels, it acts as both the reforming catalyst and the electrode [9,10]. The mechanism for partial oxidation using MoO_2 has been explained by the Mars–van Krevelen (MvK) mechanism [11,12]. In the MvK redox model, the lattice oxygen on the MoO_2 surface reacts with the hydrocarbon to form a mixture of H_2, CO, H_2O and CO_2, leaving the surface in a reduced $Mo^{(4-\delta)+}$ state together with oxygen vacancies. The reduced sites are subsequently reoxidized by the gas-phase oxygen that is fed into the system. Meanwhile, the oxygen ions that are produced by oxidizing the reduced $Mo^{(4-\delta)+}$ sites are then used to replenish the oxygen vacancies. In partial oxidation, the oxygen-to-fuel ratio needs to be controlled within a well-defined range to prevent MoO_2 being either oxidized to MoO_3 or reduced to Mo_2C. The entire redox reaction of, for instance, *n*-dodecane over MoO_2 is indicated by Eqs. (1) and (2):

$$C_{12}H_{26} + 12O^{2-} + 6Mo^{4+} \rightarrow 12CO + 13H_2 + 6Mo^{(4-\delta)+} + 6(4-\delta)e^- \quad (1)$$

$$6O_2 + 6Mo^{(4-\delta)+} + 6(4-\delta)e^- \rightarrow 12O^2 + 6Mo^{4+} \quad (2)$$

Ti-doped MoO_2 nanoparticles were synthesized to potentially address the limited oxygen-to-fuel ratio operating conditions where the catalytic redox cycle is sustained for the partial oxidation by changing the redox properties [13]. It is also desirable to avoid cell failure in SOFCs by improving the redox stability of the anodes [14]. For example, Ti-doped Sr_2NiMoO_6 was found to have increased stability in an H_2 reducing atmosphere compared to the undoped perovskite [15]. Thus Ti-doped MoO_2 has the potential as an alternative anode with enhanced redox stability in SOFCs for direct utilization of hydrocarbon fuels.

The primary objective of the present study was to determine the effect of high temperatures (i.e. the typical operating temperatures of fuel reforming and SOFCs) on the structure of Ti-doped MoO_2 and the kinetics of hydrogen reduction. For the present study, hydrogen was used to create a reducing environment for examining the redox stability of annealed Ti-doped MoO_2.

Ti-doped MoO_2 samples with a Ti/Mo atomic ratio of 0.03 were prepared by a solution-based method, as reported previously [13]. Briefly, titanium (IV) oxide bis(2,4-pentanedionate) precursor was dissolved in 99.9% methanol, and molybdenum trioxide was dissolved in 28 wt.% ammonium hydroxide. The solution containing the Mo-precursor was diluted with distilled water and then stabilized with triethanolamine. Two solutions were mixed and heated at 350 °C for 5 h, followed by calcination in air at 500 °C for 4 h to form Ti-doped MoO_3. Hydrothermal reduction was performed at 210 °C for 15 h in a Teflon-lined stainless steel autoclave with as-prepared Ti-doped MoO_3 dispersed

* Corresponding authors.; e-mail: qian.he@email.wsu.edu

http://dx.doi.org/10.1016/j.scriptamat.2014.12.012
1359-6462/

in ethylene glycol and mixed with distilled water. The final products were obtained by drying at 100 °C for 24 h. The freshly prepared undoped and Ti-doped MoO_2 samples were annealed in a quartz tube furnace from 25 to 1000 °C at 10 °C min^{-1} in flowing N_2. After annealing, the samples were cooled down naturally to 25 °C. A dopant concentration of 3 at.% was used because higher concentrations were found to exceed the solubility limit of TiO_2 in MoO_2 [13]. Undoped material was synthesized using the same approach in the absence of the titanium precursor.

X-ray diffraction (XRD) patterns of as-synthesized undoped and Ti-doped MoO_2 samples together with annealed undoped and Ti-doped MoO_2 samples were collected using Co K_α radiation in a Philips diffractometer with an iron filter. The diffractometer was operated at 40 kV and 45 mA. Transmission electron microscopy (TEM) with a Philips CM-200 electron microscope operated at 200 kV was used to provide a direct observation of changes in particle size after annealing. Surface compositional analysis was obtained by X-ray photoelectron spectrometry (XPS) using a spectrometer equipped with a Kratos AXIS-165 monochromatized Al K_α X-ray anode (1486.6 eV) and with a power of 202 W. XPS depth profile analysis was carried out by etching the surface of the sample for different times using argon ions. Infrared spectra were recorded at room temperature using a Nicolet iS50 Fourier transform infrared (FTIR) spectrometer to detect any interaction between Ti and MoO_2 in annealed Ti-doped MoO_2. Spectra were collected by averaging 128 scans at a resolution of 4 cm^{-1}. Raman spectra were recorded at room temperature on a Horiba Jobin Yvon LabRAM HR spectrometer with a resolution of 1 cm^{-1}. A diode-pumped solid-state (DPSS) Model Ventus 532 nm laser was used as the excitation source. Thermogravimetric analysis (TGA) was performed with a Mettler TGA/DSC1 instrument to study the kinetics of hydrogen reduction of annealed undoped and Ti-doped MoO_2. Nonisothermal reduction was carried out using a mixture of 10 vol.% H_2 in N_2 and by raising the temperature from 25 to 1000 °C at different heating rates (5, 10 and 15 °C min^{-1}).

The diffractograms of all the samples shown in Figure 1 can be exclusively indexed to monoclinic MoO_2 (JCPDS No. 032-0671). Within the detection limits of this technique, no other crystalline phases were found.

The diffraction patterns from the annealed samples have sharper peaks with a smaller full width at half maximum compared to those from the as-synthesized samples, indicating that heat treatment causes particle growth. TEM images of Ti-doped MoO_2 samples are shown in Figure 2(A) and (B). Before annealing, the average particle size of Ti-doped

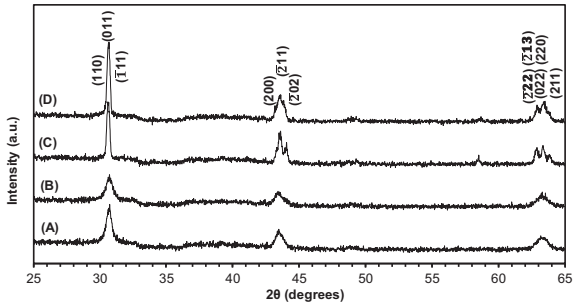

Figure 1. XRD patterns of (A) undoped MoO_2, (B) Ti-doped MoO_2, (C) annealed MoO_2 and (D) annealed Ti-doped MoO_2.

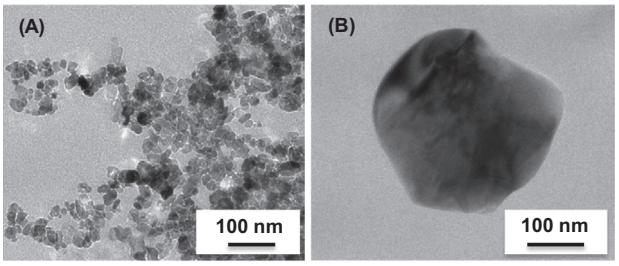

Figure 2. TEM images of (A) as-synthesized Ti-doped MoO_2 and (B) annealed Ti-doped MoO_2.

MoO_2 is ~20 nm, which is consistent with the peak broadening in the XRD pattern shown in Figure 1(B). After annealing, the particle size of the Ti-doped MoO_2 increases to ~200 nm, which agrees with the presence of sharper peaks in the XRD pattern, as shown in Figure 1(D). XPS with profile depth analysis was performed to obtain the surface composition of the annealed Ti-doped MoO_2. The results of the depth profile analysis are given in Table 1.

The carbon detected by XPS comes from organic residues formed during the synthesis process. The initial Ti/Mo ratio is ~0.104 on the surface of the annealed Ti-doped MoO_2, whereas the ratio in the as-synthesized Ti-doped MoO_2 is ~0.022 (determined previously [13]). The significantly increased Ti/Mo ratio after annealing implies Ti enrichment on the surface of the MoO_2 particles. The gradual decrease in Ti/Mo ratio with sputtering time indicates a gradient distribution of Ti within the surface layer of MoO_2.

The FTIR spectra of the annealed undoped and Ti-doped MoO_2 shown in Figure 3(A) were recorded within the 1300–700 cm^{-1} range. Absorption bands in the 1000–900 cm^{-1} range are associated with the Mo=O stretching vibrations [16]. The Mo–O–Mo stretching vibration detected at 850 cm^{-1} vanishes in the annealed Ti-doped MoO_2, indicating changes in the local environment of annealed MoO_2 upon doping. Additionally, a new feature at 761 cm^{-1} is observed in the annealed Ti-doped MoO_2. This vibration band could be due to Mo–O–Ti stretching, as observed by other groups [17]. Raman spectroscopy was used to determine the presence of TiO_2 at concentrations that cannot be detected by XRD due to its limited sensitivity. Figure 3(B) shows the Raman spectra of annealed undoped and Ti-doped MoO_2. As seen, both spectra show Raman bands associated with MoO_2 at around 991 cm^{-1} (υ_{as} Mo=O stretch), 819 cm^{-1} (υ_s Mo=O stretch), 660 cm^{-1} (υ_{as} O–Mo–O stretch), 334 cm^{-1} (δ O–Mo–O bend) and 278 cm^{-1} (δ O=Mo=O wagging) [18,19]. In the Raman spectrum of the annealed Ti-doped MoO_2, there is no indication of the presence of a discrete TiO_2 phase. However, the intensity of Mo=O terminal

Table 1. Atomic percentage and ratio of each element with sputtering time for annealed Ti-doped MoO_2.

Sputtering time (min)	Element				Ratio
	O	C	Mo	Ti	Ti/Mo
0	54.70	16.60	25.98	2.71	0.104
5	61.27	0.00	35.58	3.15	0.089
10	58.56	0.00	38.60	2.85	0.074
15	56.55	0.00	40.77	2.67	0.065

Please cite this article in press as: Q. He et al., Scripta Mater. (2015), http://dx.doi.org/10.1016/j.scriptamat.2014.12.012